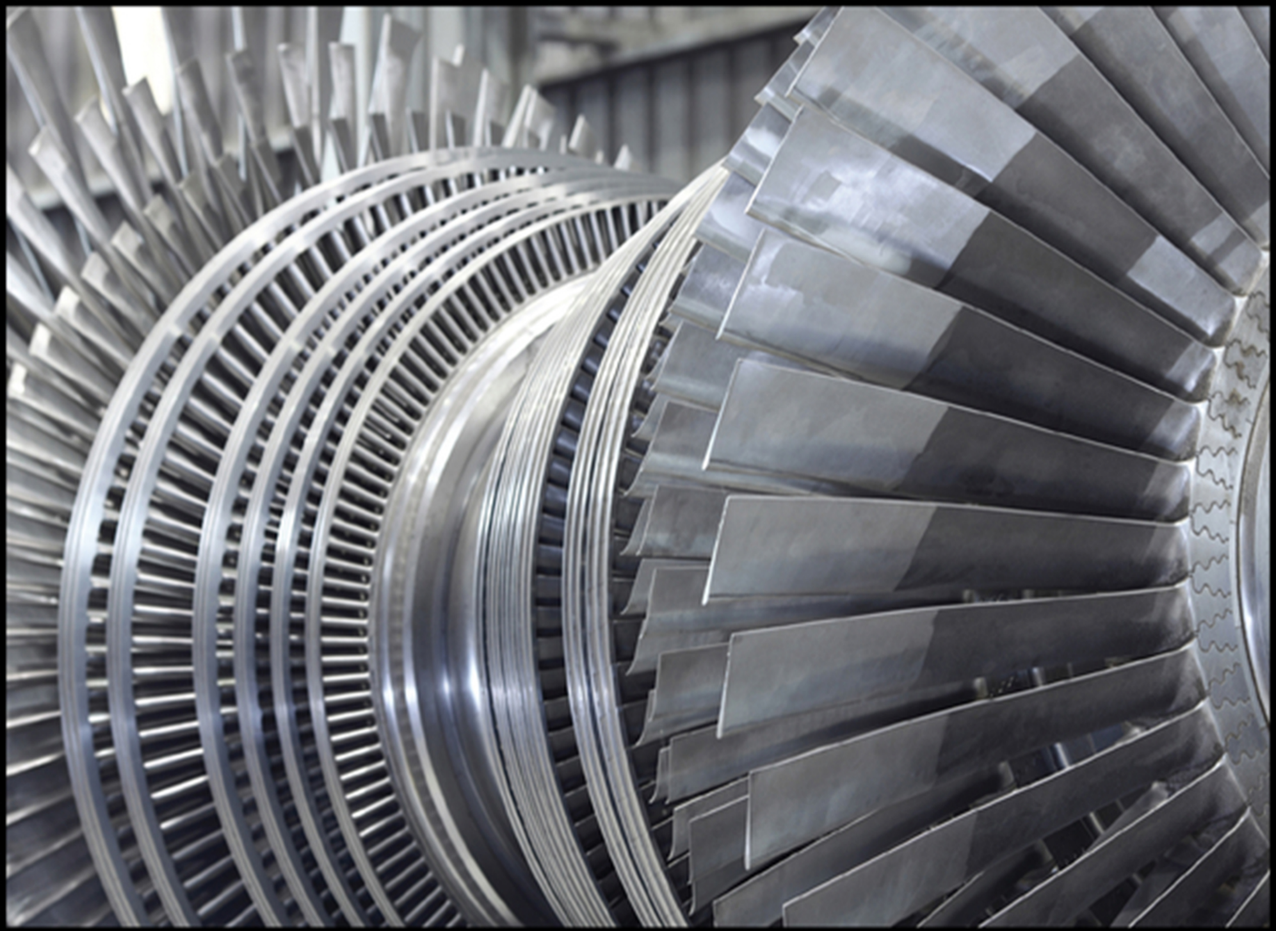

Bearing Dynamic Coefficients in Rotordynamics

Computation Methods and Practical Applications

Łukasz Breńkacz

with website

ASME PRESS

WILEY

Bearing Dynamic Coefficients in Rotordynamics

Wiley-ASME Press Series

Computer Vision for Structural Dynamics and Health Monitoring
Dongming Feng, Maria Q. Feng

Theory of Solid-Propellant Nonsteady Combustion
Vasily B. Novozhilov, Boris V. Novozhilov

Introduction to Plastics Engineering
Vijay K. Stokes

Fundamentals of Heat Engines: Reciprocating and Gas Turbine Internal Combustion Engines
Jamil Ghojel

Offshore Compliant Platforms: Analysis, Design, and Experimental Studies
Srinivasan Chandrasekaran, R. Nagavinothini

Computer Aided Design and Manufacturing
Zhuming Bi, Xiaoqin Wang

Pumps and Compressors
Marc Borremans

Corrosion and Materials in Hydrocarbon Production: A Compendium of Operational and Engineering Aspects
Bijan Kermani and Don Harrop

Design and Analysis of Centrifugal Compressors
Rene Van den Braembussche

Case Studies in Fluid Mechanics with Sensitivities to Governing Variables
M. Kemal Atesmen

The Monte Carlo Ray-Trace Method in Radiation Heat Transfer and Applied Optics
J. Robert Mahan

Dynamics of Particles and Rigid Bodies: A Self-Learning Approach
Mohammed F. Daqaq

Primer on Engineering Standards, Expanded Textbook Edition
Maan H. Jawad and Owen R. Greulich

Engineering Optimization: Applications, Methods and Analysis
R. Russell Rhinehart

Compact Heat Exchangers: Analysis, Design and Optimization using FEM and CFD Approach
C. Ranganayakulu and Kankanhalli N. Seetharamu

Robust Adaptive Control for Fractional-Order Systems with Disturbance and Saturation
Mou Chen, Shuyi Shao, and Peng Shi

Robot Manipulator Redundancy Resolution
Yunong Zhang and Long Jin

Stress in ASME Pressure Vessels, Boilers, and Nuclear Components
Maan H. Jawad

Combined Cooling, Heating, and Power Systems: Modeling, Optimization, and Operation
Yang Shi, Mingxi Liu, and Fang Fang

Applications of Mathematical Heat Transfer and Fluid Flow Models in Engineering and Medicine
Abram S. Dorfman

Bioprocessing Piping and Equipment Design: A Companion Guide for the ASME BPE Standard
William M. (Bill) Huitt

Nonlinear Regression Modeling for Engineering Applications: Modeling, Model Validation, and Enabling Design of Experiments
R. Russell Rhinehart

Geothermal Heat Pump and Heat Engine Systems: Theory and Practice
Andrew D. Chiasson

Fundamentals of Mechanical Vibrations
Liang-Wu Cai

Introduction to Dynamics and Control in Mechanical Engineering Systems
Cho W.S. To

Bearing Dynamic Coefficients in Rotordynamics

Computation Methods and Practical Applications

Łukasz Breńkacz
Institute of Fluid Flow Machinery
Polish Academy of Sciences
Gdańsk, Poland

This Work is a co-publication between John Wiley & Sons Ltd and ASME Press.

ASME PRESS

WILEY

© 2021 John Wiley & Sons Ltd
This Work is a co-publication between John Wiley & Sons Ltd and ASME Press

All rights reserved. No part of this publication may be reproduced, stored in a retrieval system, or transmitted, in any form or by any means, electronic, mechanical, photocopying, recording or otherwise, except as permitted by law. Advice on how to obtain permission to reuse material from this title is available at http://www.wiley.com/go/permissions.

The right of Łukasz Breńkacz to be identified as the author of this work has been asserted in accordance with law.

Registered Office
John Wiley & Sons, Inc., 111 River Street, Hoboken, NJ 07030, USA

Editorial Office
111 River Street, Hoboken, NJ 07030, USA

For details of our global editorial offices, customer services, and more information about Wiley products visit us at www.wiley.com.

Wiley also publishes its books in a variety of electronic formats and by print-on-demand. Some content that appears in standard print versions of this book may not be available in other formats.

Limit of Liability/Disclaimer of Warranty
While the publisher and authors have used their best efforts in preparing this work, they make no representations or warranties with respect to the accuracy or completeness of the contents of this work and specifically disclaim all warranties, including without limitation any implied warranties of merchantability or fitness for a particular purpose. No warranty may be created or extended by sales representatives, written sales materials or promotional statements for this work. The fact that an organization, website, or product is referred to in this work as a citation and/or potential source of further information does not mean that the publisher and authors endorse the information or services the organization, website, or product may provide or recommendations it may make. This work is sold with the understanding that the publisher is not engaged in rendering professional services. The advice and strategies contained herein may not be suitable for your situation. You should consult with a specialist where appropriate. Further, readers should be aware that websites listed in this work may have changed or disappeared between when this work was written and when it is read. Neither the publisher nor authors shall be liable for any loss of profit or any other commercial damages, including but not limited to special, incidental, consequential, or other damages.

Library of Congress Cataloging-in-Publication Data

Names: Breńkacz, Łukasz, author.
Title: Bearing dynamic coefficients in rotordynamics : computation methods and practical applications / Łukasz Breńkacz.
Description: First edition. | Hoboken, NJ : Wiley, 2021. | Includes bibliographical references and index.
Identifiers: LCCN 2020053700 (print) | LCCN 2020053701 (ebook) | ISBN 9781119759263 (hardback) | ISBN 9781119759249 (adobe pdf) | ISBN 9781119759171 (epub) | ISBN 9781119759287 (obook)
Subjects: LCSH: Rotors–Dynamics. | Bearings (Machinery)
Classification: LCC TJ1058 .B74 2022 (print) | LCC TJ1058 (ebook) | DDC 621.8/2–dc23
LC record available at https://lccn.loc.gov/2020053700
LC ebook record available at https://lccn.loc.gov/2020053701

Cover Design: Wiley
Cover Image: © photosoup/iStock/Getty Images

Set in 9.5/12.5pt STIXTwoText by SPi Global, Pondicherry, India

10 9 8 7 6 5 4 3 2 1

to my wife Dagmara, my daughter Agata, and my son Wojciech

Contents

List of Figures *x*
List of Tables *xvi*
Preface *xvii*
Symbols and Abbreviations *xix*
About the Companion Website *xxi*

1 Introduction *1*
1.1 Current State of Knowledge *1*
1.2 Review of the Literature on Numerical Determination of Dynamic Coefficients of Bearings *6*
1.3 Review of the Literature on Experimental Determination of Dynamic Coefficients of Bearings *7*
1.4 Purpose and Scope of the Work *10*

2 Practical Applications of Bearing Dynamic Coefficients *14*
2.1 Single Degree of Freedom System Oscillations *16*
  2.1.1 Constant excitation Force *18*
  2.1.2 Excitation by Unbalance *20*
  2.1.3 Impact of Damping and Stiffness *24*
2.2 Oscillation of Mass with Two Degrees of Freedom *26*
2.3 Cross-Coupled Stiffness and Damping Coefficients *28*
2.4 Summary *33*

3 Characteristics of the Research Subject *34*
3.1 Basic Technical Data of the Laboratory Test Rig *34*
3.2 Analysis of Rotor Dynamics *36*
3.3 Analysis of the Supporting Structure *42*
3.4 Summary *44*

4 Research Tools *46*
4.1 Test Equipment *46*
4.2 Test.Lab Software *49*
4.3 Samcef Rotors Software *51*
4.4 Matlab Software *51*

4.5 MESWIR Series Software (KINWIR, LDW, NLDW) *52*
4.6 Abaqus Software *53*

5 Algorithms for the Experimental Determination of Dynamic Coefficients of Bearings *55*
5.1 Development of the Calculation Algorithm *55*
5.2 Verification of the Calculation Algorithm on the Basis of a Numerical Model *58*
5.3 Results of Calculations of Dynamic Coefficients of Bearings *62*
5.4 Summary *64*

6 Inclusion of the Impact of an Unbalanced Rotor *65*
6.1 Calculation Scheme *65*
6.2 Definition of the Scope of Identification *67*
6.3 Results of the Calculation of Dynamic Coefficients of Bearings Including Rotor Unbalance *68*
6.4 Summary *69*

7 Sensitivity Analysis of the Experimental Method of Determining Dynamic Coefficients of Bearings *70*
7.1 Method of Carrying Out a Sensitivity Analysis *70*
7.2 Description of the Reference Model *71*
7.3 Influence of the Stiffness of the Rotor Material *71*
7.4 Influence of Uneven Force Distribution on Two Bearings *72*
7.5 Changing the Direction of the Excitation Force and its Effect on the Results Obtained *75*
7.6 Eddy Current Sensor Displacement Impact Assessment *76*
7.7 Calculation Results for an Asymmetrical Rotor *77*
7.8 Summary *79*

8 Experimental Studies *81*
8.1 Software Used for Processing of Signals from Experimental Research *82*
8.2 Software Used for Calculations of Dynamic Coefficients of Bearings *83*
8.3 Preparation of Experimental Tests *85*
8.4 Implementation of Experimental Research *87*
8.5 Processing of the Signal Measured During Experimental Tests *91*
8.6 Results of Calculations of Dynamic Coefficients of Hydrodynamic Bearings on the Basis of Experimental Research *93*
8.7 Verification of Results Obtained *98*
8.8 Summary *100*

9 Numerical Calculations of Bearing Dynamic Coefficients *102*
9.1 Method of Calculating Dynamic Coefficients of Bearings *102*
9.2 Calculation of Dynamic Coefficients of Bearings Using a Method with Linear Calculation Algorithm *107*

9.3 Calculation of Dynamic Coefficients of Bearings Using a Method with Non-linear Calculation Algorithm *113*
9.4 Verification of Results Obtained *119*
9.5 Summary *123*

10 Comparison of Bearing Dynamic Coefficients Calculated with Different Methods *125*

11 Summary and Conclusions *129*

Appendix A *134*
Appendix B *145*
Appendix C *152*
Research Funding *155*
References *156*
Index *163*

List of Figures

Figure 1.1 Lubrication film model for small journal displacement. *3*

Figure 1.2 Methods of analysis for (a) small and (b) large displacement of the journal. *6*

Figure 2.1 Bearing as part of a rotating system. Question marks indicate the places where dynamic coefficients of bearings occur. *15*

Figure 2.2 Different bearing models: (a) oscillating mass with one degree of freedom; (b) bi-directional oscillating mass (two degrees of freedom); and (c) bi-directional oscillating mass with the inclusion of cross-coupled stiffness and damping coefficients. *16*

Figure 2.3 Displacement of the mass attached to a fixed support by means of stiffness and damping coefficients as a result of a constant force. *18*

Figure 2.4 The effect of a change in the damping coefficients on the displacement of the mass point which is being acted on by a constant force. The arrows represent the direction of displacement change due to the increase of damping coefficient values. *19*

Figure 2.5 The effect of a change in the stiffness coefficients on the displacement of the mass point which is being acted on by a constant force. The arrows represent the direction of displacement change due to the decrease of stiffness coefficient values. *19*

Figure 2.6 A single degree of freedom system with harmonic excitation. *20*

Figure 2.7 The effect of a change in the damping coefficients on the displacement of the mass point which is being acted on by a constant harmonic with a frequency of 300 Hz. *21*

Figure 2.8 The effect of a change in the stiffness coefficients on the displacement of the mass point which is being acted on by a constant harmonic with a frequency of 300 Hz. *22*

Figure 2.9 Excitation force of constant value and of variable value changing along with frequency. *23*

Figure 2.10 The relationship between the excitation force frequency and the amplitude of the system response for a constant force F. *23*

Figure 2.11 The relationship between the excitation force frequency and the amplitude of the system response for the force F variable along with frequency. *24*

Figure 2.12 Impact of damping coefficients. *25*

Figure 2.13 Impact of stiffness coefficients. *25*

Figure 2.14 Impact of mass coefficients. *26*

Figure 2.15 Areas of influence of different types of coefficients for variable amplitude values of excitation force. *26*

Figure 2.16 Areas of influence of different types of coefficients for the constant amplitude of excitation force. *27*

Figure 2.17 Combination of oscillation in two directions taking into account the main stiffness and damping coefficients of the bearing. *27*

Figure 2.18 Two-directional displacement and trajectories: (a) $c_{xx} = c_{yy} = 6400\,\text{N·s/m}$; (b) $c_{xx}\cdot 2$; and (c) $c_{yy}\cdot 2$. *29*

Figure 2.19 Combination of oscillation in two directions taking into account the main and cross-coupled stiffness and damping coefficients of the bearing. *30*

Figure 2.20 Trajectory changes: (a) c_{xy} and $c_{yx} = 0\,\text{N·s/m}$; (b) $c_{xy} = 0\,\text{N·s/m}$ and $c_{yx} = 6400\,\text{N·s/m}$; and (c) $c_{xy} = 0\,\text{N·s/m}$ and $c_{yx} = 6400\,\text{N·s/m}$. *31*

Figure 2.21 Trajectory changes: (a) k_{xy} and $k_{yx} = 0\,\text{N/m}$; (b) $k_{xy} = 6\,630\,000\,\text{N/m}$ and $k_{yx} = 0\,\text{N/m}$; and (c) $k_{xy} = 0\,\text{N/m}$ and $k_{yx} = 6\,630\,000\,\text{N/m}$. *32*

Figure 3.1 Photograph of the laboratory test rig. *35*

Figure 3.2 Diagram of the laboratory test rig. *35*

Figure 3.3 (a) Hydrodynamic bearing and (b) bearing diagram. *36*

Figure 3.4 Run-up of the laboratory test rig; during 66.4 seconds the speed was increased linearly from 1000 to 8400 rpm. *37*

Figure 3.5 Maximum displacement of the rotor journals. *37*

Figure 3.6 Stable operation of bearings no. 1 (a and b) and no. 2 (c and d) at 3250 rpm; the diagrams show the signal recorded in X (a and c) and Y (b and d) directions; the short time interval (0.3 seconds) shows approximately 8 revolutions. *38*

Figure 3.7 Stable operation of bearings no. 1 (a and b) and no. 2 (c and d) at 3250 rpm; the diagrams show the signal recorded in X (a and c) and Y (b and d) directions during 10 seconds. *39*

Figure 3.8 FFT analysis of the stable operation signal from eddy current sensors bearings no. 1 (a and b) and no. 2 (c and d) at 3250 rpm; the diagrams show the signal measured in X (a and c) and Y (b and d) directions. *40*

Figure 3.9 Trajectory of bearing journal movement no. 2 during stable operation at a speed of 3250 rpm: (a) signal measured by sensors and (b) signal after filtering operation. *41*

Figure 3.10 Combination of the vibration trajectories of a second bearing operating on a laboratory test rig for (a) below resonance speed (3250 rpm), (b) close to resonance speed (4500 rpm), and (c) above resonance speed (5750 rpm). *41*

Figure 3.11 Cascade diagram based on the accelerometer signal placed on support no. 2 in the X direction (horizontal); on the drawing is highlighted the result of the FFT analysis at a rotational speed of 3000 rpm (dark gray horizontal line). *42*

Figure 3.12	The first form of natural vibrations of the laboratory test rig. *44*
Figure 4.1	SCADAS mobile analyzer. *47*
Figure 4.2	(a) Eddy current sensors placed at a 90° angle to each other and perpendicular to the rotor axis and (b) module used for processing signals from eddy current sensors – demodulator. *47*
Figure 4.3	(a) Accelerometer used to measure accelerations of vibrations of the bearing supports and (b) portable accelerometer calibrator. *48*
Figure 4.4	Impact hammer. *48*
Figure 4.5	(a) Speed measurement using a laser sensor and (b) fiber optic switch. *48*
Figure 4.6	The Vision Research Phantom v2512 camera (right), the LED lamps used for illumination (center), and the laboratory test rig (left). *49*
Figure 4.7	(a) MBJ Diamond 401 measuring device used for balancing the rotor and (b) the OPTALIGN Smart RS device for shaft alignment. *50*
Figure 4.8	Interface of the Test.Lab 11B software. *50*
Figure 4.9	Interface of the Samcef Rotors software. *51*
Figure 4.10	Interface of the Matlab software. *52*
Figure 4.11	Interface of GRAFMESWIR – a graphical processor of the NLDW software. *53*
Figure 4.12	Interface of the Abaqus/CAE software 6.14-2. *54*
Figure 5.1	(a) Rotor model in the Samcef Rotors software and (b) bearing model. *56*
Figure 5.2	Diagram for the calculation of dynamic bearing coefficients. *59*
Figure 5.3	(a) Force in direction X as a function of time and (b) displacement of bearing no. 2 as a function of time. *61*
Figure 5.4	(a) Frequency distribution of force and (b) amplitude of node no. 2 as a function of frequency. *61*
Figure 5.5	Bearing no. 1: (a) flexibility amplitude and (b) flexibility phase. *61*
Figure 5.6	The first form of natural vibrations of the rotor at 46 Hz. *62*
Figure 6.1	Calculation scheme of dynamic coefficients of bearings including unbalance. *66*
Figure 6.2	(a) Stable operation of the rotor – reference signal in the bearing and (b) amplitude of vibrations after inducing the rotor by means of a impact hammer – signal in the bearing. *66*
Figure 6.3	(a) Amplitude of vibrations after subtracting the reference signal from the excitation signal and (b) fast Fourier transform of this signal. *67*
Figure 6.4	The fast Fourier transform displacement signal in bearings for rotational speed (a) 2800 rpm and (b) 10 000 rpm. *68*
Figure 6.5	Dynamic flexibility of bearings: (a) amplitude course and (b) phase angle course. *68*
Figure 7.1	Diagram showing the sensitivity analysis scheme. *71*
Figure 7.2	(a) Rotor model on which the method of force displacement is marked. (b) Bearing response signal for the first bearing in the X direction after inducing the system in the X direction; comparison after excitation in the middle and force displaced by the value $s = 30$ mm. *73*

Figure 7.3 (a) Model showing how the force is applied at an angle and (b) the response signal of the first bearing in the X and Y directions after excitation at an angle of $\alpha = 0°$ and $\alpha = 15°$. *75*

Figure 7.4 Model on which the place of bearing displacement measurement was marked (systems with p indexes) and places taken into account during calculation of dynamic coefficients of bearings (means of bearing housings). *77*

Figure 7.5 Diagram of an asymmetrical rotor. *78*

Figure 7.6 Response of an asymmetrical rotor system. *78*

Figure 8.1 Program window for signal preparation; the diagrams presented the data read for a signal corresponding to a speed of 4500 rpm and excitation in the Y direction. *83*

Figure 8.2 Window of the software used for calculations of dynamic coefficients of bearings. *84*

Figure 8.3 Photograph showing the test stand during the shaft alignment. *86*

Figure 8.4 Photograph showing the tested rotor. *86*

Figure 8.5 Phantom Camera Control, a program window for operating a high-speed camera; a fragment of the recording of inducing the rotor with a impact hammer can be seen in the background. *87*

Figure 8.6 Calculation scheme of dynamic coefficients of bearings. *88*

Figure 8.7 Signal measured near bearing no. 2 in the Y direction at 4500 rpm and excitation with a impact hammer in the Y direction. *89*

Figure 8.8 Excitation force curve in the Y direction over 20 seconds; signal stored at 4500 rpm. *89*

Figure 8.9 Excitation force in the X and Y directions over 0.4 ms; excitation at 4500 rpm. (a) Values not reset outside the main peak and (b) signal with resetting. *90*

Figure 8.10 Stable bearing operation no. 2 (a and b) at 4500 rpm and signal after excitation (c and d); the graphs show the displacements in the X direction (a and c) and Y direction (b and d); the time of the signal shown in the graphs is 0.1 seconds. *91*

Figure 8.11 Amplitude of rotor vibrations after excitation in the X and Y directions for the first (a) and second (b) bearings; the reference signal has been subtracted from the signal after the excitation. *92*

Figure 8.12 Changes in the stiffness coefficients of bearing no. 2 for the entire speed range. *97*

Figure 8.13 Changes in the damping coefficients of bearing no. 2 for the entire speed range. *97*

Figure 8.14 Changes in the mass coefficients of bearing no. 2 for the entire speed range. *97*

Figure 8.15 Increasing vibration amplitude recorded in bearing no. 2 during operation at 4000 rpm after excitation with an impact hammer in the Y direction. *98*

Figure 8.16 Schematic model of mass, damping, and stiffness. *99*

Figure 8.17 Comparison of the dynamic response of the real rotor and the numerical model (the model takes into account the experimentally determined stiffness and damping coefficients). *99*
Figure 9.1 Coordinate system at a selected point in the lubrication gap. *103*
Figure 9.2 Algorithm of calculation of a radial hydrodynamic bearing. *108*
Figure 9.3 Numerical rotor model in the KINWIR program. *109*
Figure 9.4 Numerical model of hydrodynamic bearing. *110*
Figure 9.5 Presentation of the pressure distribution calculated for the static equilibrium point at a speed of 3250 rpm in the Kinwir program. *110*
Figure 9.6 Bearing no. 2 stiffness coefficients calculated using a linear algorithm in the KINWIR program. *112*
Figure 9.7 Bearing no. 2 damping coefficients calculated using a linear algorithm in the KINWIR program. *112*
Figure 9.8 Numerical model of the rotor, bearing and disk in the NLDW program. *113*
Figure 9.9 Pressure distribution calculated using the NLDW program for (a–d) 4 journal positions (in 90° increments) at 3250 rpm. *114*
Figure 9.10 Stiffness coefficients calculated in the NLDW program for 3 rotor revolutions at a rotational speed of 3250 rpm. *116*
Figure 9.11 Damping coefficients calculated in the NLDW program for 3 rotor revolutions at a speed of 3250 rpm. *116*
Figure 9.12 Stiffness coefficients calculated in the NLDW program for 3 rotor revolutions at a rotational speed of 3750 rpm. *117*
Figure 9.13 Damping coefficients calculated in the NLDW program for 3 rotor revolutions at a speed of 3750 rpm. *117*
Figure 9.14 Stiffness coefficients calculated in the NLDW program for 3 rotor revolutions at a rotational speed of 5500 rpm. *118*
Figure 9.15 Damping coefficients calculated in the NLDW program for 3 rotor revolutions at a speed of 5500 rpm. *118*
Figure 9.16 Bearing journal displacements calculated using the method with a linear calculation algorithm. *119*
Figure 9.17 Bearing journal displacements calculated using the NLDW program. *120*
Figure 9.18 Vibration trajectories of the journal of bearing no. 2: (a) measured during experimental tests: (b) calculated using a linear algorithm: and (c) calculated using the NLDW program. *121*
Figure 9.19 The FFT analysis of the signal for a speed of 5750 rpm based on experimental tests in the direction of (a) X and (b) Y; analogous results calculated numerically for the linear algorithm in the direction of (c) X and (d) Y; calculations by means of a non-linear algorithm in the NLDW program in the direction of (e) X and (f) Y. *122*
Figure 10.1 (a) Change in journal vibration trajectory due to e.g. increased rotor unbalance or changes in bearing parameters (trajectory 1, 2, or 3). (b) Trajectory after inducing a bearing operating at a static equilibrium point (O_c). A model showing the assumptions of linear operation of the

system. (c) Trajectory after excitation during operation with a larger ellipse of vibrations. The dotted line shows a sample trajectory after excitation in point Ow. After a short time, the rotor journal returns to the previous constant ellipse on which it was moving earlier (shown by a continuous line). *127*

Figure 11.1 A diagram of the work carried out. The division into experimental tests and numerical analyses and the relationships between the various chapters and sections of the monograph are indicated. *130*

Figure A.1 Fast Fourier transform (FFT) diagrams of the first and second bearings in the X and Y directions for rotational speeds of 2250–3000 rpm. *135*

Figure A.2 FFT diagrams of the first and second bearings in the X and Y directions for rotational speeds of 3250–4000 rpm. *136*

Figure A.3 FFT diagrams of the first and second bearings in the X and Y directions for rotational speeds of 4250–5000 rpm. *137*

Figure A.4 FFT diagrams of the first and second bearings in the X and Y directions for rotational speeds of 5250–6000 rpm. *138*

Figure A.5 Vibration trajectory of the first bearing for 16 rotational speeds, from 2250 to 6000 rpm. *139*

Figure A.6 Vibration trajectory of the second bearing for 16 rotational speeds, from 2250 to 6000 rpm. *140*

Figure A.7 Cascade diagram of an accelerometer placed on support no. 1 in the X direction (horizontal). *141*

Figure A.8 Cascade diagram of an accelerometer placed on support no. 1 in the Y direction. *141*

Figure A.9 Cascade diagram of an accelerometer placed on support no. 2 in the X direction. *142*

Figure A.10 Cascade diagram of an accelerometer placed on support no. 2 in the Y direction. *142*

Figure A.11 Shaft alignment report – part one. *143*

Figure A.12 Shaft alignment report – part two. *144*

Figure C.1 Vibration trajectories calculated for the second bearing using a linear algorithm based on the KINWIR and LDW programs. *153*

Figure C.2 Vibration trajectories calculated for the second bearing using a non-linear algorithm in the NLDW program. *154*

List of Tables

Table 3.1 Successive eigenfrequencies and the corresponding damping values calculated for the laboratory test rig. *43*
Table 5.1 Parameters of the numerical model. *59*
Table 5.2 Stiffness coefficients. *60*
Table 5.3 Damping coefficients. *60*
Table 5.4 Mass coefficients. *63*
Table 7.1 Summary of the real and calculated stiffness, damping and mass coefficients for the two bearings for the reference case; representation of the relative calculations error. *72*
Table 7.2 Summary of the real and calculated stiffness, damping, and mass coefficients for the two bearings for a case with displaced force; results “with correction” take into account the uneven distribution of excitation force in the calculation procedure. *74*
Table 7.3 Summary of the real and calculated stiffness, damping and mass coefficients for the two bearings for a case with an excitation at an angle of $\alpha = 15°$. *76*
Table 7.4 Summary of the real and calculated stiffness, damping and mass coefficients of two bearings for an asymmetrical rotor. *78*
Table 8.1 Stiffness, damping and mass coefficients of the rotor–bearing system for the entire speed range. *95*
Table 8.2 Standard deviation of stiffness, damping and mass coefficients of the rotor – bearing system for the entire speed range. *96*
Table 9.1 Parameters of the numerical model in the KINWIR program. *109*
Table 9.2 Stiffness and damping coefficients obtained from linear calculations in the KINWIR. *111*
Table 9.3 Minimum and maximum values of stiffness coefficients (N/m) calculated in the NLDW program. *115*
Table 9.4 Minimum and maximum values of damping coefficients (N·s/m) calculated in the NLDW program. *115*
Table 10.1 Comparison of the calculated stiffness and damping coefficients for the three methods used for a speed of 3000 rpm. *126*